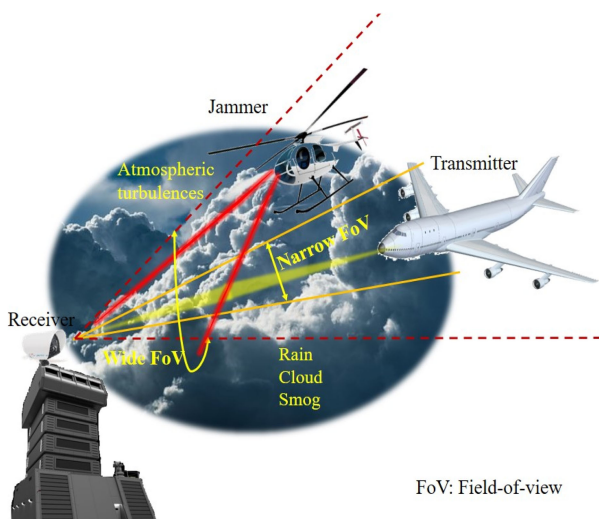🔓 **Open Access**

Alleviation of Jamming in Free Space Optical Communication over Gamma-Gamma Channel with Pointing Errors

Pratiti Paul, *Student Member, IEEE*
Manav R. Bhatnagar, *Senior Member, IEEE*
Anshul Jaiswal, *Student Member, IEEE*

FoV: Field-of-view

Alleviation of Jamming in Free Space Optical Communication over Gamma-Gamma Channel with Pointing Errors

Pratiti Paul [ID] **, *Student Member, IEEE*,**
Manav R. Bhatnagar [ID] **, *Senior Member, IEEE*,**
and Anshul Jaiswal [ID] **, *Student Member, IEEE***

Department of Electrical Engineering, Indian Institute of Technology Delhi, New Delhi
110016 India

Abstract: In this paper, the groundwork on jamming effect and its alleviation mechanisms in free space optical (FSO) communication are studied over Gamma-Gamma (GG) fading channels along with the pointing error (PE) effects. A closed-form expression of the bit error rate (BER) is evaluated analytically for a single-input single-output (SISO) FSO system in the presence of jammer. The worst case jamming condition for maximization of error is calculated numerically. The jammer channel is considered to be GG distributed. Being the most dominating noise, the jamming signal is acted as the only noise source in the considered FSO set-up. Therefore, this study is performed over additive GG noise channel. The error performances are investigated for different atmospheric turbulence (AT) regimes (weak to strong) and for different PE parameters of jamming noise. Moreover, to combat the jamming effect, a multiple-input single-output (MISO) FSO system is considered. A closed-form expression of the BER of the multiple transmit channels over the GG noise is analytically calculated. The analytical results for both SISO and MISO FSO systems are verified with the help of the simulation results obtained by MATLAB software. It is established that MISO FSO performs better than SISO FSO system in terms of BER performance under the influence of jamming noise. Furthermore, many important observations are made upon the BER performances for different AT and PE parameters for SISO and MISO FSO systems.

Index Terms: Bit error rate (BER), free space optical (FSO) communication, Gamma-Gamma (GG) fading, GG noise, jamming, optimization, pointing error (PE), signal-to-jamming ratio (SJR).

1. Introduction

Recently, free space optical (FSO) communication has put its valuable signature in high speed wireless communication society. This state of the art research in this field has established several notable advantages like unlicensed frequency spectrum and low implementation cost [1], [2].

Moreover, the application of multiple-input multiple-output (MIMO) technology improved the performance of FSO systems in terms of better diversity gain, improved bandwidth utilization, and larger coverage area [3]–[7]. Regardless of the advancements–the FSO communication system has achieved in terms of performance improvement [8]–[22], the safety and authenticity is yet to be verified firmly in order to establish a successful and secure communication. The unguided nature of FSO communication system makes it highly interruptible by unauthorized users with mischievous intentions, which is very dangerous for military application or any other security-constrained protocol [23]. There are two important parameters needed to be considered while studying the jamming phenomenon–operating frequency and field-of-view (FoV) of the application. The effects of jamming and different anti-jamming strategies have been studied by leaps and bounds for radio frequency (RF) communication [24]–[27], where the jammer needs to radiate the signal over a wide ranges of frequencies to jam the RF network. On the other hand, there exist very limited number of wavelengths, reserved for the FSO communication. Moreover, the spectral width of the laser beam used in FSO communication system, is very narrow, mostly restricted around a specific wavelength value (1300 nm or 1550 nm). Therefore, the operating frequency is very much predictable and can be hampered by an intruder effortlessly.

FoV is a parameter which can be defined as the solid angle through which the receive photo-detector is open to the incoming optical signals from the transmitter. In most of the FSO applications, the FoV of the optical detector is kept wide [2]. Wider FoV helps to defeat the pointing error (PE) problem and to maximize the acceptance rate of transmitted optical signal. The FSO communication can be broadly classified in two major fields–terrestrial FSO communication and satellite FSO communication. In terrestrial communications like in backhaul networks, the requirement of large aperture diameter is necessary to receive most of the scintillating optical signal, which in turn leads to an wider FoV [2]. Further, aperture averaging, a vital mechanism, is performed in FSO backbone networks [28]–[31]. In mobile FSO communication systems where the transceivers are in motion and also in satellite communications, the FoV needs to be significantly broad. There are several practical applications which comply the purpose of broader FoV.

- The National Aeronautics and Space Administration (NASA) is working on the ingenious technologies [32] for long distance interplanetary optical communications, where the optical receiver sensor which collects the useful information from the planetary system through optical path needs a broad FoV with high resolution factors.
- In [33]–[38], the future mobile FSO communication and FSO in space [39] claim for broad FoV for maximization of detected signal and effective tracking capability.
- The Connectivity Lab of Facebook has launched solar-powered drones, Aquila [40], [41], which are mobile in nature and connected with each other via optical link [42]–[44]. For that, Facebook has developed an optical detector with high FoV [40, Fig. 1].
- In project Loon, the Google's Internet balloons are mobile and they communicate via FSO links, leading to a requirements of wider FoV [45]–[47].

If any established FSO communication is hampered by a jamming attack, then it becomes very difficult to detect the original transmitted data at the receiving end. This annoying and sometimes harmful intrusion lead to the Denial-of-Services (DoS) in the wireless optical network [23]. So, with the enormous advancement of the FSO communication technology and its application, the malicious effects from the adversaries are also needed to be investigated. Further, it is needed to study the response of the jammed system in terms of error performances and to develop mitigation process diligently to negate the adverse effect of jamming. Broadly two types of jammer can be defined in a communication network with variable transmit power, transmitting opportunistically to jam the receiver: (i) *Constant Jammer:* Remains in the on-state all the time and constantly impinges its constant power until or unless all of its power gets exhausted. (ii) *Pulse Jammer:* It makes use of its energy whenever there is an authorized signal passing through the channel, thus altering its on and off phases. Due to the randomness of the jammimg activity, the received signal becomes very unpredictable at the receiver.

In FSO communication system, due to maximization of the acceptance rate of the incoming signal, a wider FoV is required. So it is quite easy for a jammer to reside inside the FoV in order
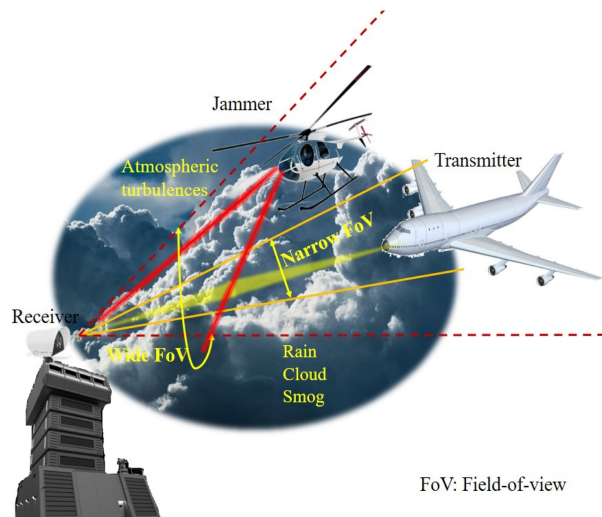
Fig. 1. FSO Receiver with narrow and wide field-of-view.

to the jamming signal to be trapped inside the photodetector as shown in Fig. 1. It is important to get the insight of the overall performances of any FSO communication system to get an idea about error occurrences due to a jammer. However, in [48], the secrecy rate of MISO FSO system is performed numerically with different non-jamming protocols in the presence of a legitimate user and an eavesdropper. However, the effects of atmospheric turbulence (AT) and PE are not taken into account. Whereas in [49]–[51], in presence of eavesdroppers the security improvement based on secret key sharing, security risks analysis through a non-line-of-sight (NLOS) scattering channel, and secure FSO employing multipath transmission by data fragmentation are studied, respectively. Although the effects of PE are not considered here. The spectrum analysis of a secure chaotic optical wireless communication systems is discussed in [52]. However, none of the aforementioned studies have considered the effect of jamming and how it affects the BER performances of FSO systems. For the first time to the best of our knowledge, the channel model of an FSO system with jammer and its mitigation in order to improve the BER are studied with combined effect of AT and PE, in this paper.

The novel contributions of this work are as follows:
- We first study the SISO FSO system considering the jamming effect over GG fading channel with PE effect. This study is based on an additive GG noise channel.
- A closed-form expression of the BER of a SISO FSO link is derived with jamming effect for all ranges of AT (from weak to strong). From the derived BER, diversity order and coding gain of the FSO system due to jammer are calculated.
- The worst case jamming is evaluated which is responsible for maximizing BER to optimize the transmitted signal power.
- For alleviation of jamming effect, the MISO FSO system performances are analyzed in terms of BER for different values of PE, worst case jamming, diversity order, and coding loss, and compared with the SISO FSO system.

Some significant observations are made from the analysis and the graphs which are provided accordingly and have not been acknowledged till date. It is also identified that by employing additional spatial dimensions to the authorized user channel, the effect of jamming can be reduced significantly.

The rest of the paper is arranged as follows. Section II provides the system and channel model of the considered FSO system with jammer and fundamental definitions related to the error performances. Section III demonstrates the mathematical analysis of SISO FSO system under the jamming effect. In Section IV, the method of jamming alleviation is described in detail.

The numerical results are discussed in Section V and some remarkable conclusions are drawn in Section VI.

2. Preliminaries

2.1 System Model

Consider an FSO link with a single transmit aperture (LASER) which emits an On-Off Keying (OOK) modulated optical signal, x, a single receive aperture (photo detector), and a malicious jammer, which tries to destroy the legitimate communication link at the receiver end, by sending optical signal by varying its power opportunistically. Moreover, the legitimate optical channel is affected by AT and PE which can deteriorate the established LOS link between the transmitter and receiver as shown in Fig. 1. Similarly, the jamming link is also affected by the AT and PE. At the receiving end, after converting the optical signal into electrical signal, the system input-output (I/O) relation can be written as:

$$y = \mathrm{R}\sqrt{E_x}h_x x + \mathrm{R}\sqrt{N_J}h_J S_J n_J + e, \tag{1}$$

where E_x denotes the peak transmit energy of the legitimate transmitter and, h_x and h_J are the fading coefficients of user and jammer channel, respectively. At the receiver, a photodiode of responsivity R is used, whose value is considered as 1; e is the additive white Gaussian noise (independent and identically distributed over each symbol duration) with zero mean and N_o variance.

The state of jammer: The injected jamming signal is denoted as n_J, whose value is considered as unity. Let us consider a random variable (RV) S_J, that captures the mode of jamming; S_J follows the Bernoulli distribution, which indicates that it has only two modes of operations–either on or off. In on state, the jammer transmits an optical signal over an OOK symbol period with probability ρ, whereas it remains idle with probability $(1 - \rho)$. Therefore, the probability distribution of S_J is given by [24]:

$$P(S_J = 1) = \rho; \quad P(S_J = 0) = 1 - \rho, \tag{2}$$

where ρ is the demographic term defining the degree of jamming activity ($\rho \in (0, 1]$) and $P(\cdot)$ denotes the probability. Let, E_J be the average jamming energy, limited in each symbol interval. However, to be precise, whenever the jammer starts invading, it transmits with energy $N_J = E_J/\rho$, the net contributing jamming energy.

At high transmit signal power region, the jamming noise is the most dominating noise than the additive white Gaussian noise. However, to be precise, the instantaneous signal-to-jamming-plus-noise (SJNR) ratio conditioned over the user and jammer channel coefficients (the jammer is in active state) can be expressed as:

$$\gamma_{g1} = \frac{h_x^2 E_x}{h_J^2 E_J/\rho + N_o}. \tag{3}$$

When the jammer is in idle state, then the signal-to-noise ratio (SNR) is given by:

$$\gamma_{g2} = \frac{h_x^2 E_x}{N_o}. \tag{4}$$

2.2 Optical Channel Model

In this paper, the effects of both AT and PE are studied in the performance evaluation of the considered system. The GG fading distribution for h_k, $k \in \{x, J\}$ can be defined as [12]:

$$f_{h_k}(h_k) \triangleq \frac{\alpha_k \beta_k \zeta_k^2}{A_0 \Gamma(\alpha_k)\Gamma(\beta_k)} G_{1,3}^{3,0}\left(\frac{\alpha_k \beta_k h_k}{A_0} \middle| \begin{array}{c} \zeta_k^2 \\ \zeta_k^2, \alpha_k - 1, \beta_k - 1 \end{array}\right), \tag{5}$$

where $G_{m,n}^{p,q}(\cdot|)$ denotes the Meijer-G function [53].

TABLE 1
AT Parameters [2], [54]

Turbulence Region	α_k	β_k	σ_{lk}^2
Weak	5.4	3.77	0.6
Moderate	4.0	1.9	1.6
Strong	4.2	1.4	3.5

Considering the plane wave nature of optical radiation, the values of AT parameters α_k and β_k can be defined as [9]:

$$\alpha_k \triangleq \frac{1}{e^{0.49\sigma_{lk}^2/\left(1+1.11\sigma_{lk}^{12/5}\right)^{7/6}} - 1}, \beta_k \triangleq \frac{1}{e^{0.51\sigma_{lk}^2/\left(1+0.69\sigma_{lk}^{12/5}\right)^{5/6}} - 1}, \tag{6}$$

where $\sigma_{lk}^2 = 1.23C_{nk}^2 \nu^{7/6} L_k^{11/6}$, characterizes the log irradiance variance, $\nu = 2\pi/\lambda$, λ is the wavelength, L_k denotes the FSO propagation path length, and C_{nk}^2 is the refractive index structure parameter.

The effect of PE can be described as the following terms, which are assimilated in (5): $A_0 = [\text{erf}(v)]^2$, $v = \sqrt{\pi/2}a/\omega_b$, $\zeta_k = \omega_{zeq}^2/2\sigma_k^2$, a denotes the radius of the receive aperture, ω_b expresses the beam-waist from center of the aperture (radius calculated at e^{-2}), $\omega_{zeq}^2 = \omega_b^2\sqrt{\pi}\text{erf}(v)/(2v\exp(-v^2))$, is the equivalent beam width, σ_k is the jitter standard deviation, and erf(.) is the error function [53]. The PE parameter, ζ_k is inversely proportional to σ_k. Thus, lesser weight of ζ_k represents a larger PE severity. The AT parameters for different regions are listed in Table 1. The turbulence parameters for strong and moderate AT conditions are available in [2], whereas, for weak turbulence condition, log irradiance variance $\sigma_{lk}^2 = 0.6$ and propagation path length parameter $L_k = 3$ KM are considered for calculation of the AT parameters using the relationship between AT parameters and σ_{lk}^2 [2, p. 141], [54].

2.3 Bit Error Rate

BER is an important performance metric to study the efficiency of any communication system. A generalized BER expression in presence of jammer can be written as:

$$P_e = P(J = on)[P(x = 0)P(error|x = 0) + P(x = 1)P(error|x = 1)]$$
$$+ P(J = off)[P(x = 0)P(error|x = 0) + P(x = 1)P(error|x = 1)], \tag{7}$$

where J denotes the state of the jammer here. Thus from (3) and (4), (7) can be written as [24]:

$$P_e = \rho P_e(\gamma_{g1}) + (1 - \rho)P_e(\gamma_{g2}), \tag{8}$$

where the first and second terms of (8) define the BER for jammer in on and off state as a function of SJNR and SNR, respectively. In (8), $P_e(\gamma_{g2})$ approaches towards zero as SNR increases (practically at the operating zone). Therefore, jamming noise is the only effective noise term at the high SNR region. Additionally, at high transmit power, the SJNR leads to:

$$\gamma_{g1} = \frac{h_x^2 E_x}{h_J^2 E_J/\rho + N_o} \approx \frac{\rho h_x^2 E_x}{h_J^2 E_J} = \rho \frac{h_x^2}{h_J^2}\gamma_J. \tag{9}$$

In (9), γ_J stands for the signal-to-jammer ratio (SJR). Fig. 2 illustrates the comparison between SJR and SNJR for different values of N_o. From the figure, it is observed that the SJR value is independent of noise power N_o. However, the decreasing noise power (i.e., when $N_o < 0$ dB or unit variance point) denotes the high SNJR region, and SNJR converges to SJR in that region, which proves validity of the assumption drawn in (9). For performing this convergence test, the user and jammer channel gains are considered to be unity and white Gaussian noise power is varied around the unit variance reference point.
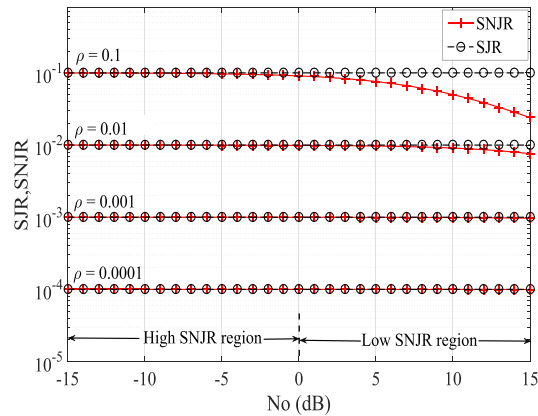
Fig. 2. Comparison between SNJR and SJR for different values of N_o with unit signal and jammer energies.

Therefore, a precise BER expression of the considered system is given by:

$$P_e \approx \rho P_e(\gamma_J). \tag{10}$$

From (10), it is anticipated that all the following performance evaluations are needed for a study over the additive Gamma-Gamma noise channel, which is different from the conventional additive Gaussian noise channel.

2.4 Diversity Order and Coding Gain

The diversity order of a communication system describes the ability of a system to reduce the effect of AT and PE due to fading, i.e., the gradient with which the BER versus SJR curve moves asymptotically at higher SJR region. Coding gain designates the additional signal power desired to obtain the same BER. At very high SJR region, the BER expression can be mathematically expressed as:

$$\lim_{\gamma_J \to \infty} \mathrm{BER}(\gamma_J) \propto (C_g \gamma_J)^{-\delta}, \tag{11}$$

where δ and C_g denotes the diversity order and coding gain, respectively.

3. Performance Metrics of SISO FSO Link Over GG Fading in Presence of Jammer

In this section, the BER performance is conducted for the considered SISO FSO system under jamming. For mathematical simplicity, we assume $\alpha_x = \alpha_J = \alpha$ and $\beta_x = \beta_J = \beta$.

3.1 ABER Evaluation

Let us first define an RV, $z \triangleq \sqrt{\frac{E_J}{\rho}} h_J$, where h_J is GG distributed, so from (5) the probability density function (PDF) of h_J is:

$$f_{h_J}(h_J) = \frac{\alpha \beta \zeta_J^2}{A_0 \Gamma(\alpha) \Gamma(\beta)} G_{1,3}^{3,0} \left(\frac{\alpha \beta h_J}{A_0} \middle| \begin{matrix} \zeta_J^2 \\ \zeta_J^2, \alpha - 1, \beta - 1 \end{matrix} \right). \tag{12}$$

Performing transformation of RV [55] and some algebra on (12), the PDF of z can be calculated as:

$$f_z(z) = \frac{\alpha \beta \zeta_J^2}{\sqrt{E_J/\rho} A_0 \Gamma(\alpha) \Gamma(\beta)} G_{1,3}^{3,0} \left(\frac{\alpha \beta z}{\sqrt{E_J/\rho} A_0} \middle| \begin{matrix} \zeta_J^2 \\ \zeta_J^2, \alpha - 1, \beta - 1 \end{matrix} \right) U(z), \tag{13}$$

where $U(.)$ denotes the unit step function.

Now, neglecting the additive Gaussian noise term in (1), we get $z = y - \sqrt{E_x}h_x x$; hence, (13) becomes:

$$f_y(y|\sqrt{E_x}, h_x, x) = \frac{\alpha\beta\zeta_J^2}{\sqrt{E_J/\rho}A_0\Gamma(\alpha)\Gamma(\beta)} G_{1,3}^{3,0}\left(\frac{\alpha\beta(y - \sqrt{E_x}h_x x)}{\sqrt{E_J/\rho}A_0}\middle| \begin{matrix} \zeta_J^2 \\ \zeta_J^2, \alpha - 1, \beta - 1 \end{matrix}\right)U(z). \quad (14)$$

Equation (14) can be expanded further in two conditions given as:

$$f_y(y) = \begin{cases} \dfrac{\alpha\beta\zeta_J^2}{\sqrt{E_J/\rho}A_0\Gamma(\alpha)\Gamma(\beta)} G_{1,3}^{3,0}\left(\dfrac{\alpha\beta y}{\sqrt{E_J/\rho}A_0}\middle| \begin{matrix} \zeta_J^2 \\ \zeta_J^2, \alpha - 1, \beta - 1 \end{matrix}\right)U(z), & \text{for } x = 0, \\[2em] \dfrac{\alpha\beta\zeta_J^2}{\sqrt{E_J/\rho}A_0\Gamma(\alpha)\Gamma(\beta)} G_{1,3}^{3,0}\left(\dfrac{\alpha\beta(y - \sqrt{E_x}h_x)}{\sqrt{E_J/\rho}A_0}\middle| \begin{matrix} \zeta_J^2 \\ \zeta_J^2, \alpha - 1, \beta - 1 \end{matrix}\right)U(z), & \text{for } x = 1. \end{cases} \quad (15)$$

Considering that the jammer is present and using (7), we can write the expression of instantaneous BER as:

$$P_{e_{SISO}}(\gamma_J, h_x) = \rho\left[0.5\int_{th}^{\infty} f_y(y|x=0)dy + 0.5\int_0^{th} f_y(y|x=1)dy\right], \quad (16)$$

where threshold $th = \sqrt{E_x}h_x$. Employing (5) and [56, Eq. (2.24.1.1)] in (16), we have:

$$P_{e_{SISO}}(\gamma_J) = \frac{\rho\zeta_x^2\zeta_J^2(\sqrt{\rho\gamma_J})^{-1}}{2(\Gamma(\alpha)\Gamma(\beta))^2} G_{5,5}^{3,4}\left(\frac{1}{\sqrt{\rho\gamma_J}}\middle| \begin{matrix} 0, -\zeta_J^2, -\alpha, -\beta, \zeta_x^2 \\ \zeta_x^2 - 1, \alpha - 1, \beta - 1, -\zeta_J^2 - 1, -1 \end{matrix}\right). \quad (17)$$

3.2 Diversity Order and Coding Gain Analysis

Under low noise condition, the BER is dominated by the smallest exponent of γ_J. Thus the smallest exponent, i.e., the diversity order of SISO FSO system can be evaluated by representing (17) using series form of the Meijer-G function [53], [57]:

$$P_{e_{SISO}} = \frac{\rho^{1/2}\zeta_x^2\zeta_J^2}{2\sqrt{\gamma_J}(\Gamma(\alpha)\Gamma(\beta))^2} \sum_{h=1}^{3} \frac{\prod_{j=1}^{3}\Gamma(q_j - q_h)\prod_{j=1}^{4}\Gamma(1 + q_h - p_j)}{\prod_{j=4}^{5}\Gamma(1 + q_h - q_j)\prod_{j=5}\Gamma(p_j - q_h)}(\sqrt{\rho\gamma_J})^{-q_h}$$

$$\times \sum_{n=0}^{\infty} \frac{(1 + q_h - p_1)_n....(1 + q_h - p_5)_n}{n!(1 + q_h - q_1)_n..,*,..(1 + q_h - q_5)_n}(\sqrt{\rho\gamma_J})^{-n}, \quad (18)$$

where $\{p\}=\{0, -\zeta_J^2, -\alpha, -\beta, \zeta_x^2\}$ and $\{q\} = \{\zeta_x^2 - 1, \alpha - 1, \beta - 1, -\zeta_J^2 - 1, -1\}$, '*' denotes the omission of hth term, $\Gamma(.)$ and $(.)_n$ denote the Gamma function and Pochhammer symbol, respectively [53]. In order to calculate diversity order the higher degrees of SJR will be neglected, hence, the by putting $n = 0$ and performing the minimization of the exponent of γ_J on (18), the asymptotic BER is given as:

$$P_{e_{SISO}} = \frac{\rho^{1/2}\zeta_x^2\zeta_J^2}{2\sqrt{\gamma_J}(\Gamma(\alpha)\Gamma(\beta))^2} \sum_{h=1}^{3} \frac{\prod_{j=1}^{3}\Gamma(q_j - q_h)\prod_{j=1}^{4}\Gamma(1 + q_h - p_j)}{\prod_{j=4}^{5}\Gamma(1 + q_h - q_j)\prod_{j=5}\Gamma(p_j - q_h)}(\sqrt{\rho\gamma_J})^{-q_h}. \quad (19)$$

From (19), we can calculate the diversity order of the system as:

$$\delta_{SISO} = \frac{1}{2}\cdot\min\{\zeta_x^2, \alpha, \beta\}. \quad (20)$$

thus the coding gain will be (with $q_{h_{min}} = 2\delta_{SISO} - 1$):

$$C_{g_{SISO}} = \left(\frac{\rho^{1-\delta_{SISO}}\zeta_x^2\zeta_J^2}{2(\Gamma(\alpha)\Gamma(\beta))^2} \frac{\prod_{j=1}^{3}\Gamma(q_j - q_{h_{min}})\prod_{j=1}^{4}\Gamma(1 + q_{h_{min}} - p_j)}{\prod_{j=4}^{5}\Gamma(1 + q_{h_{min}} - q_j)\prod_{j=5}\Gamma(p_j - q_{h_{min}})}\right)^{-1/\delta_{SISO}}. \quad (21)$$

Let ρ_1 and $(\rho_2 \geqslant \rho_1)$ are the jamming probabilities. Now, we can write the relative coding gain of the system from (21) as:

$$\Delta C_{g_{SISO}} = \left(\frac{\rho_2}{\rho_1}\right)^{1-1/\delta_{SISO}}.$$

(22)

3.3 Worst Case Jamming Probability ρ^*_{SISO}

Now, we consider that the jammer knows the channel parameters of the legitimate link, so it will try to utilize the communication channel tactfully to maximize the error rate. Therefore, in the worst case scenario, the value of the degree of jamming ρ can be found by differentiating (17) with respect to (w.r.t.) ρ and setting it to zero. For the purpose of finding the optimal SJR value, let us define a variable, $u \triangleq 1/\sqrt{\rho\gamma_J}$; differentiating (17) w.r.t. ρ by using [58], and employing change of variables and the chain rule, we have:

$$\frac{dP_{e_{SISO}}(\gamma_J)}{d\rho} = \left[\frac{\rho^{-7/2}\zeta_x^2\zeta_J^2}{4(\Gamma(\alpha)\Gamma(\beta))^2\gamma_J^{3/2}} G_{5,5}^{3,4}\left(\frac{1}{\sqrt{\rho\gamma_J}} \middle| \begin{matrix} 0, -\zeta_J^2, -\alpha, -\beta, \zeta_x^2 \\ \zeta_x^2 - 1, \alpha - 1, \beta - 1, -\zeta_J^2 - 1, -1 \end{matrix} \right) \right]$$

$$+ \left[\frac{\rho^{-1}\zeta_x^2\zeta_J^2}{4(\Gamma(\alpha)\Gamma(\beta))^2\gamma_J} G_{6,6}^{3,5}\left(\frac{1}{\sqrt{\rho\gamma_J}} \middle| \begin{matrix} -1, -\zeta_J^2 - 1, -\alpha - 1, -\beta - 1, \zeta_x^2 - 1 \\ \zeta_x^2 - 2, \alpha - 2, \beta - 2, 0, -2 - \zeta_J^2 - 1, -2 \end{matrix} \right) \right].$$

(23)

From (23), it can be seen that it is very complex to find a closed-form expression of optimal ρ. So, optimal value of ρ, for SISO system, i.e., ρ^*_{SISO}, for the worst case jamming can be expressed numerically (approximately calculated from Fig. 6) as:

$$\rho^*_{SISO} = \begin{cases} 1, & \text{for } \gamma_J \leqslant 25.12, \\ \frac{25.12}{\gamma_J}, & \text{for } \gamma_J > 25.12. \end{cases}$$

(24)

Thus the ABER expression in worst case jamming is same as (17) under the condition of $\gamma_J \leqslant 25.12$. But for $\gamma_J > 25.12$, the ABER expression approximately is given by:

$$P^*_{e_{SISO}} = \frac{0.2}{\gamma_J}$$

(25)

Remark 1: These observations affirm the inverse relationship between the worst case jamming and SJR when SJR is greater than 14 dB. Additionally, they disclose the fact that a jammer requires its power to be condensed in a smaller interval of time in the higher SJR region.

4. Alleviation of Jamming Effect

In this section, the study of error performance evaluation in presence of jammer is extended to a general MISO FSO system. The notion of using multiple transmit apertures at the source end envisions the fact that the FSO system will now get a chance to transmit the legitimate information to the receiver over multiple channels. Moreover, it is well known that MISO FSO system can be used to improve the system performance in terms of diversity order. Therefore, it motivates to study the behavior of a MISO ($N_t \times 1$) FSO system when there is a jammer, always present to interrupt the dedicated communication link by making the receiver congested. For the considered set-up, the I/O relation is given as:

$$y' = R \sum_{i=1}^{N_t} \frac{\sqrt{E_x}}{N_t} h_{x_i} x + R\sqrt{N_J} h_J S_J n_J,$$

(26)

where, h_{x_i} is the gain of corresponding FSO channels, E_x is the total transmit energy and the value of responsivity R is 1. Let us define a variable, $z' \triangleq \sqrt{N_J} h_J$ hence, from (26), we have: $z' = y' - \sum_{i=1}^{N_t} \frac{\sqrt{E_x}}{N_t} h_{x_i} x$.

4.1 ABER Calculation

By using transformation of RV and putting the value of z' in (13), the PDF of output signal y' can be expressed as:

$$
f_{y'}(y') = \begin{cases}
\dfrac{\alpha\beta\zeta_J^2}{\sqrt{E_J/\rho}A_0\Gamma(\alpha)\Gamma(\beta)} G_{1,3}^{3,0}\left(\dfrac{\alpha\beta y'}{\sqrt{E_J/\rho}A_0} \middle| \begin{matrix}\zeta_J^2 \\ \zeta_J^2, \alpha-1, \beta-1\end{matrix}\right) U(z'), & \text{for } x=0, \\[3ex]
\dfrac{\alpha\beta\zeta_J^2}{\sqrt{E_J/\rho}A_0\Gamma(\alpha)\Gamma(\beta)} G_{1,3}^{3,0}\left(\dfrac{\alpha\beta\left(y'-\sum_{i=1}^{N_t}\frac{\sqrt{E_x}}{N_t}h_{x_i}\right)}{\sqrt{E_J/\rho}A_0} \middle| \begin{matrix}\zeta_J^2 \\ \zeta_J^2, \alpha-1, \beta-1\end{matrix}\right) U(z'), & \text{for } x=1.
\end{cases}
\tag{27}
$$

From (7) and (27), and $h_{sum} = \sum_{i=1}^{N_t} h_{x_i}$ we get:

$$
P_{e_{SISO}}(\gamma_J, h_{sum}) = \frac{\rho\alpha\beta\zeta_J^2\sqrt{\rho\gamma_J}h_{sum}}{2N_t A_0\Gamma(\alpha)\Gamma(\beta)} G_{2,4}^{4,0}\left(\frac{\alpha\beta\sqrt{\rho\gamma_J}h_{sum}}{N_t A_0} \middle| \begin{matrix}\zeta_J^2, 0 \\ -1, \zeta_J^2-1, \alpha-1, \beta-1\end{matrix}\right).
\tag{28}
$$

To find the joint distribution of N_t channels, the moment generating function (MGF) approach is used. The MGF of h_{x_i} is given by:

$$
M_{h_{x_i}}(s) = \int_0^\infty e^{-sz'} f_{h_{x_i}}(z')dz'.
\tag{29}
$$

Thus, the MGF of h_{x_i} can be expressed as [13]:

$$
M_{h_{x_i}}(s) = Q_o s^{-\zeta_x^2} + \sum_{n=0}^\infty R_n s^{-n-\alpha} + \sum_{n=0}^\infty S_n s^{-n-\beta},
\tag{30}
$$

where Q_o, R_n, and S_n are defined in [13, Eq. (20)]. Considering the independent channels, the MGF of h_{sum} can be written as:

$$
M_{h_{sum}}(s) = \prod_{i=1}^{N_t} M_{h_{x_i}}(s) = (M_{h_{x_i}}(s))^{N_t}.
\tag{31}
$$

From (30) and (31) and after some algebra using trinomial expansion [59], we have:

$$
M_{h_{sum}}(s) = \sum_{\substack{k_1,k_2,k_3 \\ k_1+k_2+k_3=N_t}} \binom{N_t}{k_1,k_2,k_3}\left(Q_o s^{-\zeta_x^2}\right)^{k_1}\left(\sum_{n=0}^\infty R_n s^{-n-\alpha}\right)^{k_2}\left(\sum_{n=0}^\infty S_n s^{-n-\beta}\right)^{k_3}
$$

$$
= \sum_{\substack{k_1,k_2,k_3 \\ k_1+k_2+k_3=N_t}} \binom{N_t}{k_1,k_2,k_3}\sum_{n=0}^\infty C_n(k_1,k_2,k_3)s^{-n-k_1\zeta_x^2-k_2\alpha-k_3\beta}.
\tag{32}
$$

The co-efficients in (32) can be computed from [53, Eq. (0.316)]. Applying inverse Laplace transformation on (32), the joint PDF of MISO FSO channel can be evaluated as:

$$
f_{h_{sum}}(z') = \sum_{\substack{k_1,k_2,k_3 \\ k_1+k_2+k_3=N_t}} \binom{N_t}{k_1,k_2,k_3}\sum_{n=0}^\infty C_n(k_1,k_2,k_3)\frac{z'^{(n+k_1\zeta_x^2+k_2\alpha+k_3\beta-1)}}{\Gamma(n+k_1\zeta_x^2+k_2\alpha+k_3\beta)}.
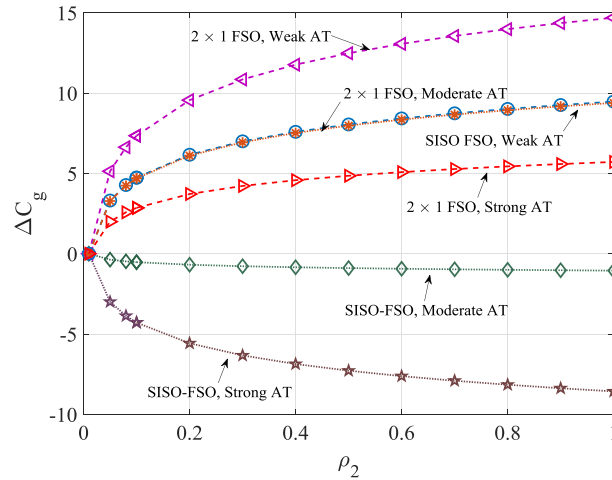\tag{33}
$$

Fig. 3. Coding gain of SISO and 2×1 FSO system in different AT region for $\rho_1 = 0.01$, $\zeta_x = 4.5856$, and $\zeta_J = 0.8545$.

Now, using (7), (28), (33), [56, Eqs. (8.2.2.15), (2.24.2.2), and (2.24.2.3)], and after some rigorous mathematics, we have the final closed-form expression of the ABER as:

$$
P_{e_{MISO}} = \frac{\zeta_J^2}{2\Gamma(\alpha)\Gamma(\beta)} \sum_{\substack{k_1,k_2,k_3 \\ k_1+k_2+k_3=N_t}} \binom{N_t}{k_1,k_2,k_3} \sum_{n=0}^{\infty} C_n(k_1,k_2,k_3) \frac{1}{\Gamma(n + k_1\zeta_x^2 + k_2\alpha + k_3\beta)}
$$

$$
\times \left(\frac{\alpha\beta}{A_o N_t}\right)^{-n-k_1\zeta_x^2-k_2\alpha-k_3\beta} \left(\sqrt{\gamma_J}\right)^{-n-k_1\zeta_x^2-k_2\alpha-k_3\beta} (\rho)^{-n/2-k_1\zeta_x^2/2-k_2\alpha/2-k_3\beta/2+1}
$$

$$
\times \left[aG_{3,5}^{4,1}\left(a\left|\begin{matrix} 0, a_1, a_2 \\ b_1, b_2, b_3, b_4, -1 \end{matrix}\right.\right) + aG_{3,5}^{5,0}\left(a\left|\begin{matrix} a_1, a_2, 0 \\ -1, b_1, b_2, b_3, b_4 \end{matrix}\right.\right) \right],
\tag{34}
$$

where a is an arbitrary positive number (considered $a = 3$ here), taken as upper and lower limit while using [56, Eqs. (2.24.2.2) and (2.24.2.3), respectively] and $a_1 = \zeta_J^2 + n + k_1\zeta_x^2 + k_2\alpha + k_3\beta$, $a_2 = n + k_1\zeta_x^2 + k_2\alpha + k_3\beta$, $b_1 = -1 + n + k_1\zeta_x^2 + k_2\alpha + k_3\beta$, $b_2 = \zeta_J^2 - 1 + n + k_1\zeta_x^2 + k_2\alpha + k_3\beta$, $b_3 = \alpha - 1 + n + k_1\zeta_x^2 + k_2\alpha + k_3\beta$, and $b_4 = \beta - 1 + n + k_1\zeta_x^2 + k_2\alpha + k_3\beta$.

4.2 Diversity Order and Coding Gain Analysis

Ignoring all the higher order terms of SJR in (34), the diversity order can be expressed as:

$$
\delta_{MISO} = \frac{N_t}{2} \cdot \min\left\{\zeta_x^2, \alpha, \beta\right\}.
\tag{35}
$$

From (34), in high SJR region, and considering ρ_1 and ($\rho_2 \geqslant \rho_1$), we can write the relative coding gain of the MISO FSO system as:

$$
\Delta C_{g_{MISO}} = \left(\frac{\rho_2}{\rho_1}\right)^{1-1/\delta_{MISO}}.
\tag{36}
$$

Remark 2: From (20), we can observe that the diversity order of the SISO FSO system is dependent on minimum value of AT and PE parameters. Also, coding gain parameter acts differently in various AT regions. In Fig. 3, the relative coding gain of the SISO FSO system is shown using (22), where it can be seen that with increasing jamming probability, the relative coding gains under strong and moderate AT region decrease, i.e., it signifies the coding losses in high SJR region. Interestingly, under weak AT condition, improvement in the relative coding gain is observed. This
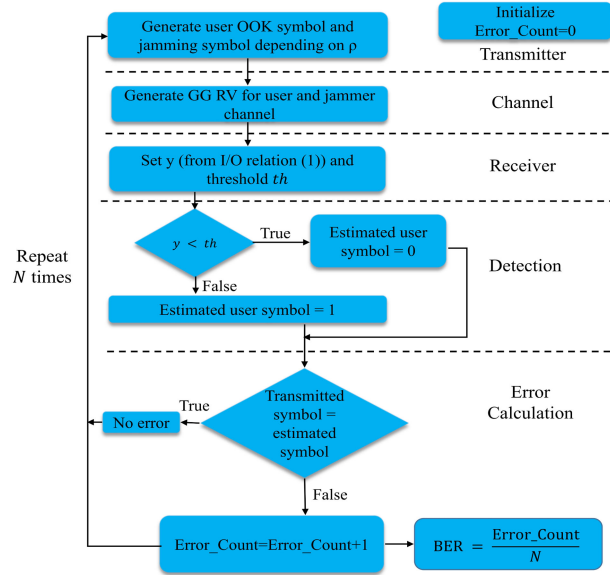
Fig. 4. Simulation flowchart.

happens because under the weak AT condition, the jammer acts as a pulse jammer and it will be further elaborated in Section V (cf. Fig. 6).

Remark 3: For MISO FSO system, the diversity order is increased by the factor of N_t, i.e., the number of transmit apertures. But for all AT regions and from (36) the system poses a relative coding gain in presence of jammer, where for weak AT it is maximum and for strong AT it is minimum as shown in Fig. 3.

4.3 Worst Case Jamming Probability ρ^*_{MISO}

Now, it is very difficult to analyze the worst case jamming probability by differentiating (34) with respect to ρ. Therefore, the optimum value of jamming probability, ρ^*_{MISO} for the worst case jamming can be evaluated numerically (approximately calculated from Fig. 9) as:

$$\rho^*_{MISO} = \begin{cases} 1, & \text{for } \gamma_J \leqslant 100, \\ \frac{100}{\gamma_J}, & \text{for } \gamma_J > 100. \end{cases} \tag{37}$$

Thus the ABER expression in worst case jamming is same as (34) under the condition of $\gamma_J \leqslant 100$. But for $\gamma_J > 100$, the expression is approximately given by:

$$P^*_{e_{MISO}} = \frac{0.35}{\gamma_J} \tag{38}$$

Remark 4: Similar to SISO case, the jammer takes its worst form when the SJR is greater than 20 dB.

5. Numerical Results and Discussions

In this section, the performances of SISO and MISO FSO systems affected by jammer are discussed in terms of BER. The studies are done for wide ranges of AT incorporating the effect of PE. The theoretical analyses are validated by the simulated results computed using MATLAB software. Figure 4 demostrates the flowchart of Monte Carlo simulation process performed for a given per symbol SJR value. The PE parameters are taken as $\zeta_x = 4.5856$ for the legitimate user and
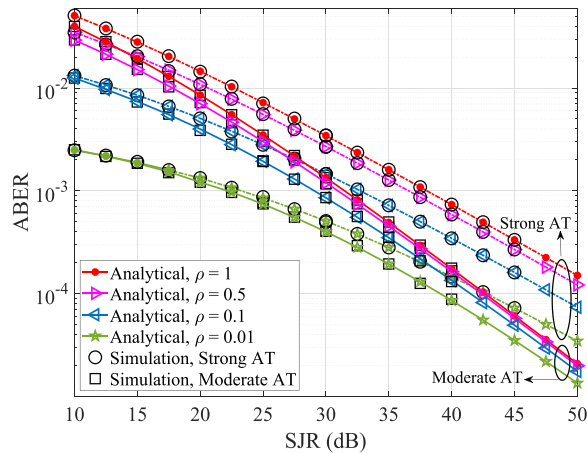
Fig. 5. Analytical and simulation ABER versus SJR graph for SISO FSO system for strong and moderate AT, various ρ, $\zeta_x = 4.5856$, and $\zeta_J = 0.8545$.
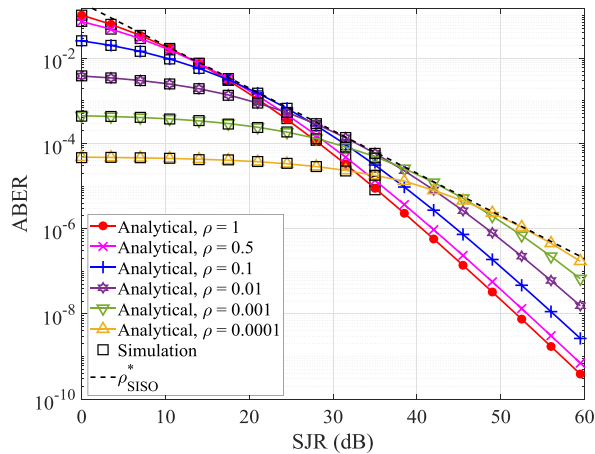

Fig. 6. Analytical and simulation ABER versus SJR graph for SISO FSO system for weak AT, various ρ, $\zeta_x = 4.5856$, and $\zeta_J = 0.8545$.

$\zeta_J = 0.8545$ for the jammer as it suffers from a more severe PE than the user. Although jamming effect are observed for different PE parameters and for various degrees of jamming ρ.

5.1 SISO FSO System Response Under Jamming Environment

From (17), Fig. 5 gives the ABER versus SJR performances of SISO FSO system for strong and moderate AT for different values of ρ. It is observed that the error performances of SISO system is poor even if at high SJR region. It can also be noticed that for both AT regions the BER graphs become parallel at high SJR region. Though the nature of error performances changes dramatically in weak AT region shown in Fig. 6. Crossovers are observed at different SJR values for different ρ. From the figure, the value of ρ^*_{SISO} expressed in (24) can be numerically calculated. It can be observed that at around 14 dB, the ABER curve for probability $\rho = 0.5$ crosses ABER curve for $\rho = 1$ and gives the worse error performances than $\rho = 1$ case from 14 dB onwards. Therefore, the jamming probability, $\rho = 1$ gives the worst error performances before 14 dB, whereas after 14 dB onwards ρ^*_{SISO} decreases with increasing SJR. From (24), it can also be noticed that when $\gamma_J = 52.5\ dB$, the worst ABER performance is obtained for probability $\rho = 0.0001$ (ρ^*_{SISO}), which
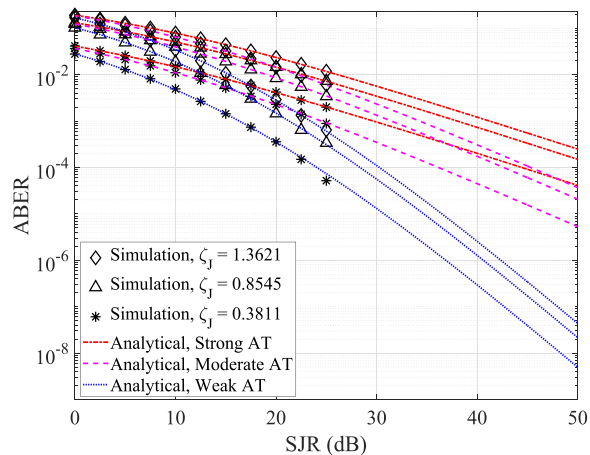
Fig. 7. Comparison between analytical and simulation ABER versus SJR graph for SISO FSO system for fixed values of $\rho = 1$ and $\zeta_x = 4.5856$.

can also be verified from the figure. Also, substituing the corresponding values of FSO system parameters (AT and PE) and ρ^*_{SISO} for paticular SJR value, the worst case ABER, (25) is derived from (17). Moreover, the difference between the BER curves of constant jammer and worst case jammer (for ρ^*) increases with SJR increment. This is because the jamming power is inversely proportional to ρ, and a low probable jammer tries to concentrate all its power to fewer symbol periods than a highly probable jammer. This behavior shows a dominating effect at high SJR values. Thus it validates the fact drawn in Remark 1.

Remark 5: The ABER performances of SISO FSO system confirms that for strong and moderate AT the worst case jamming will occur when $\rho = 1$, but in weak AT the worst case jamming is depicted by ρ^*.

Figure 7 shows the effect of PE parameters on ABER graphs. It can be seen that the higher the value of PE parameter ζ_J (signifies better alignment, less PE) of the jammer, the poor will be the error performances as it affects the authorized communication link destructively.

5.2 Convergence Test

The ABER expression in (34) incorporates the infinite terms of summation ($0 \leq n \leq \infty$), hence it is needed to find out the limit of the summation terms so that the expression becomes convergent. Let us consider that the ABER converges for a finite number of summation terms, i.e., k_l, the abridged value of the infinite summation. This convergence test is shown in Fig. 8. For all the AT regions, it is observed from Fig. 8 that ABER converges for a finite value of k_l and follows the actual ABER slope. It can also be observed from the figure that for all AT regions, the larger the value of k_l, the better is the convergence of ABER. At a value of $k_l = 15$, the convergence starts from 22.5 dB, 26 dB, 29 dB for strong, moderate, and weak ATs respectively, i.e., all ABER plots start converging from the operating ranges of transmit power. Thus for a better convergence performance the value of k_l is taken as 25 for all the following figures of ABER of MISO FSO system.

5.3 Towards Alleviation of Jamming by Increasing the Spatial Dimensions

In the aforementioned sections, we have discussed the severity of jamming in the considered SISO FSO system and the poor BER performances in presence of jammer. Therefore, to mitigate the extremity of jamming the MISO FSO setup is studied. Also, the performance comparisons between SISO and MISO FSO system are provided here under the jamming attack.
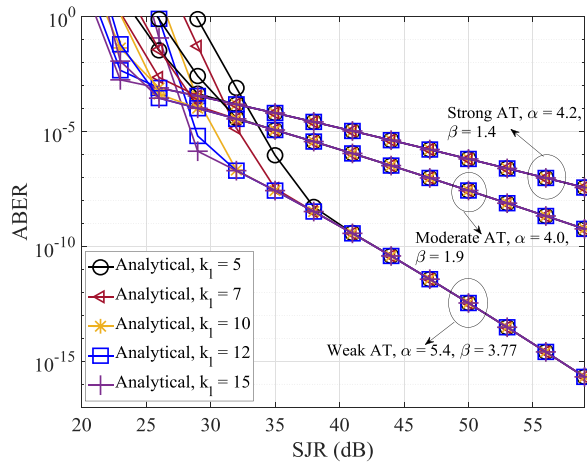
Fig. 8. Convergence graph for different values of k_l under strong, moderate, and weak AT regions (for $\rho = 1$).
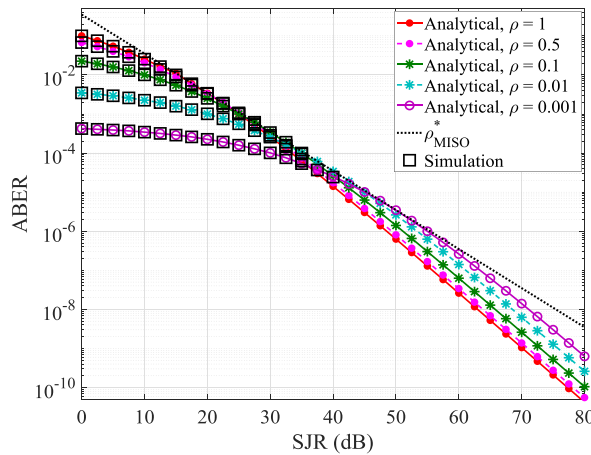

Fig. 9. Analytical and simulation ABER versus SJR graph for MISO (2×1) FSO system for strong AT, various ρ, $\zeta_x = 4.5856$, and $\zeta_J = 0.8545$.

Figure 9 demonstrates the ABER performances for 2×1 MISO FSO system in the strong AT regime. Here, it can be observed that the crossovers in ABER plots are appeared in the strong AT region. It is now quite obvious and can also be envisioned easily that the similar nature will also appear in ABER curves under moderate and weak AT region. From Fig. 5, it is seen that the error performance of SISO FSO system is very poor in strong AT region in presence of jammer compared to 2×1 FSO system shown in Fig. 9. For example, under the constant jamming and $\rho = 1$, at 50 dB the ABER of the SISO FSO system (cf. Fig. 5) is 1.5×10^{-4} but for 2×1 FSO system it is 6.3×10^{-7}. Again, to get the ABER of 3×10^{-5} when ρ changes from 0.01 to 1, the difference between required transmit power is 7 dB less in 2×1 MISO FSO system, which will further decrease with increasing number of transmit apertures. It also indicates that the difference between the worst case jammer (ρ^*_{MISO}) and jammer with fixed power gradually increases for higher values of SJR. Therefore, at high SJR region the injected jamming power is required to be condensed into the smaller portion of time.

Figure 10 depicts the error performance comparison between the SISO and 2×1 MISO FSO system in strong AT region for different PE parameters of jamming link. From the figure it is seen that the ABER performance is significantly improved and even for small PE of jamming link the
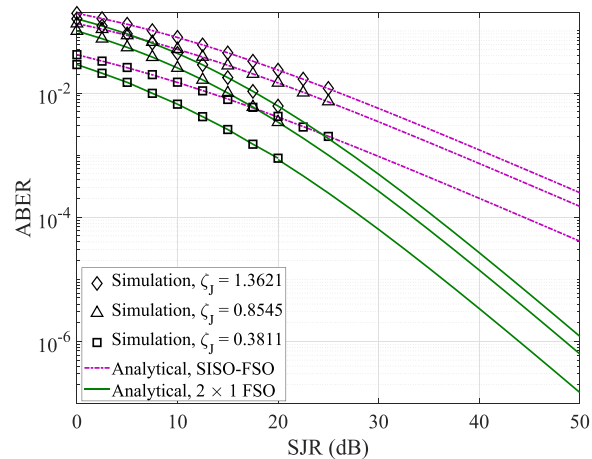
Fig. 10. Comparison between analytical and simulation ABER versus SJR graph for MISO (2×1) FSO system under strong AT for fixed values of $\rho = 1$ and $\zeta_x = 4.5856$.
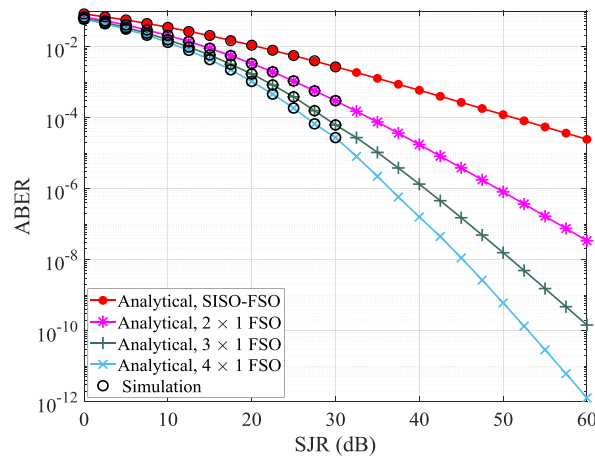

Fig. 11. Comparison between analytical and simulation ABER versus SJR graph for MISO ($N_t \times 1$) FSO link under strong AT for fixed values of $\rho = 0.5$, $\zeta_x = 4.5856$, and $\zeta_J = 0.8545$.

error decreases more rapidly in the 2×1 FSO system. To achieve ABER of 2.5×10^{-4} and at $\zeta_J = 1.3621$, i.e., even with low PE severity of the jammer, the required transmit power for 2×1 FSO system is 17.5 dB less than SISO FSO system.

Remark 6: It is now established that the MISO FSO system is significantly capable to tolerate the impact of jamming. In 2×1 MISO FSO system (cf. Fig. 9), the crossovers are arising under the strong AT region whereas it is not the case in SISO FSO system under strong AT region. It happens in the case of MISO FSO system because there are more than one transmit channels available for communication even under the strong AT condition. Therefore, the probability of getting all the channels in deep fade is very small, i.e., all MISO FSO channels remain mostly favorable to be detected efficiently around the mean value of the joint PDF. Moreover, under different PE parameters the performance improvement in MISO FSO system is quite symbolic.

In Fig. 11, the BER performances for MISO FSO system are shown by varying the number of transmit apertures. It can be observed from the figure that when the number of transmit apertures increases, the ABER performance improves notably. If the diversity order is calculated at high SJR region (between 50 and 60 dB), then it can also be observed that the diversity order is 0.7, 1.4, 2.03,

and 2.7 (considering $\min\{\zeta_x^2, \alpha, \beta\} = \beta$ here) for SISO and MISO (N_t = 2, 3, and 4, respectively) FSO systems, correspondingly. Therefore, the diversity order improves gradually with increasing number of transmit apertures. Hence, we can also verify the diversity order of both SISO and MISO FSO system which is derived analytically in (20) and (35) from infinite series representation of ABER given in (19) and (34), respectively.

6. Conclusion

The jamming effect in FSO communication system has been studied in this paper, where both the legitimate and jammer channels have been considered to experience the GG fading with PE effect. The poor performances of the SISO FSO system in terms of BER have been analyzed and observed over the additive GG noise. To reduce the effect of jamming in FSO communication, a MISO FSO system has been analytically studied. All derivations are obtained over additive non-Gaussian noise channel, which poses the system model and signal detection process uniquely distinct from the additive Gaussian noise based FSO system. For SISO and 2×1 FSO systems, the worst case jamming has been evaluated numerically, and it has been observed that it carries an inverse relation with SJR. Interestingly, in low SJR region, the worst system performance has been noticed for an always on jammer, i.e., $\rho = 1$; whereas, a random jammer with a small jamming probability, e.g. $\rho = 0.001$ induces more error in high SJR region. This observation also reveals the pulse nature of jamming effect, which demonstrates that at high SJR region a low probable jammer affects the FSO system worstly. However, it has been established analytically that a MISO FSO system performs significantly better than a SISO FSO system when there is jamming in the communication channel.

References

[1] L. Andrews and R. L. Philips, *Laser Beam Propagation Through Random Media*. Bellingham, WA, USA: SPIE, 2005.
[2] Z. Ghassemlooy, W. Popoola, and S. Rajbhandari, *Optical Wireless Communications System and Channel Modelling With MATLAB*. Boca Raton, FL, USA: CRC Press, 2013.
[3] E. Bayaki, R. Schober, and R. K. Mallik, "Performance analysis of MIMO free-space optical systems in gamma-gamma fading," *IEEE Trans. Commun.*, vol. 57, no. 11, pp. 3415–3424, Nov. 2009.
[4] N. Letzepis and A. G. Fabregas, "Outage probability of the Gaussian MIMO free-space optical channel with PPM," *IEEE Trans. Commun.*, vol. 57, no. 12, pp. 3682–3690, Dec. 2009.
[5] T. A. Tsiftsis, H. G. Sandalidis, G. K. Karagiannidis, and M. Uysal, "Optical wireless links with spatial diversity over strong atmospheric turbulence channels," *IEEE Trans. Wireless Commun.*, vol. 8, no. 2, pp. 951–957, Feb. 2009.
[6] M. R. Bhatnagar, "Differential decoding of SIM DPSK over FSO MIMO links," *IEEE Commun. Lett.*, vol. 17, no. 1, pp. 79–82, Jan. 2013.
[7] H. Moradi, H. H. Refai, and P. G. LoPresti, "Circular MIMO FSO nodes with transmit selection and receive generalized selection diversity," *IEEE Trans. Veh. Technol.*, vol. 61, no. 3, pp. 1174–1181, Mar. 2012.
[8] K. P. Peppas and C. K. Datsikas, "Average symbol error probability of general-order rectangular quadrature amplitude modulation of optical wireless communication systems over atmospheric turbulence channels," *IEEE/OSA J. Opt. Commun. Netw.*, vol. 2, no. 2, pp. 102–110, Feb. 2010.
[9] W. O. Popoola and Z. Ghassemlooy, "BPSK subcarrier intensity modulated free-space optical communications in atmospheric turbulence," *IEEE/OSA J. Lightw. Technol.*, vol. 27, no. 8, pp. 967–973, Apr. 2009.
[10] M. Uysal, J. Li, and M. Yu, "Error rate performance analysis of coded free-space optical links over gamma-gamma atmospheric turbulence channels," *IEEE Trans. Wireless Commun.*, vol. 5, no. 6, p. 1229–1233, Jun. 2006.
[11] X. Liu, "Free-space optics optimization models for building sway and atmospheric interference using variable wave-length," *IEEE Trans. Commun.*, vol. 57, no. 2, pp. 492–498, Feb. 2009.
[12] W. Gappmair, "Further results on the capacity of free-space optical channels in turbulent atmosphere," *IET Commun.*, vol. 5, no. 9, pp. 1262–1267, Jun. 2011.
[13] M. R. Bhatnagar and Z. Ghassemlooy, "Performance analysis of gamma-gamma fading FSO MIMO links with pointing errors," *IEEE/OSA J. Lightw. Technol.*, vol. 34, no. 92, pp. 2158–2169, Feb. 2016.
[14] Z. Wang, W. Zhong, S. Fu, and C. Lin, "Performance comparison of different modulation formats over free-space optical (FSO) turbulence links with space diversity reception technique," *IEEE Photon. J.*, vol. 1, no. 6, pp. 277–285, Dec. 2009.
[15] H. S. Khallaf, H. M. H. Shalaby, J. M. Garrido-Balsells, and S. Sampei, "Performance analysis of a hybrid QAM-MPPM technique over turbulence-free and gamma-gamma free-space optical channels," *IEEE/OSA J. Opt. Commun. Netw.*, vol. 9, no. 2, pp. 161–171, Feb. 2017.
[16] A. Jaiswal and M. R. Bhatnagar, "Free-space optical communication: A diversity-multiplexing tradeoff perspective," *IEEE Trans. Inf. Theory*, vol. 65, no. 2, pp. 1113–1125, Feb. 2019.

[17] J. Park, E. Lee, and G. Yoon, "Average bit-error rate of the Alamouti scheme in gamma-gamma fading channels," *IEEE Photon. Technol. Lett.*, vol. 23, no. 4, pp. 269–271, Feb. 2011.

[18] M. R. Bhatnagar and S. Anees, "On the performance of Alamouti scheme in gamma-gamma fading FSO links with pointing errors," *IEEE Wireless Commun. Lett.*, vol. 4, no. 1, pp. 94–97, Feb. 2015.

[19] E. Bayaki and R. Schober, "On space-time coding for freespace optical systems," *IEEE Trans. Commun.*, vol. 58, no. 1, pp. 58–62, Jan. 2010.

[20] X. Song and J. Cheng, "Subcarrier intensity modulated MIMO optical communications in atmospheric turbulence," *IEEE/OSA J. Opt. Commun. Netw.*, vol. 5, no. 9, pp. 1001–1009, Sep. 2013.

[21] M. Abaza, R. Mesleh, A. Mansour, and H. A. Aggoune, "Diversity techniques for FSO communication system in correlated log-normal channels," *Opt. Eng.*, vol. 53, no. 1, Jan. 2014, Art. no. 016102.

[22] M. Safari and M. Uysal, "Do we really need OSTBCs for free-space optical communication with direct detection?," *IEEE Trans. Wireless Commun.*, vol. 7, no. 11, pp. 4445–4448, Nov. 2008.

[23] S. S. D. Neo, Free space optics communication for mobile military platforms. Calhoun. 2003. [Online]. Available: https://calhoun.nps.edu/handle/10945/6160. Accessed on: Oct. 2018.

[24] S. Park and W. E. Stark, "Performance analysis of concatenated convolutional codes for STBC systems in pulse jamming," in *Proc. IEEE Mil. Commun. Conf.*, 2014, pp. 1510–1515.

[25] S. Amuru, H. S. Dhillon, and R. M. Buehrer, "On jamming against wireless networks," *IEEE Trans. Wireless Commun.*, vol. 16, no. 1, pp. 412–428, Jan. 2017.

[26] Q. Yan, H. Zeng, T. Jiang, M. Li, W. Lou, and Y. T. Hou, "Jamming resilient communication using MIMO interference cancellation," *IEEE Trans. Inf. Forensics Security*, vol. 11, no. 7, pp. 1486–1499, Jul. 2016.

[27] K. Grover, A. Lim, and Q. Yang, "Jamming and anti-jamming techniques in wireless networks: A survey," *Int. J. Ad Hoc Ubiquitous Comput.*, vol. 17, no. 4, pp. 197–215, Dec. 2014.

[28] D. L. Fried, "Aperture averaging of scintillation," *OSA J. Opt. Soc. Amer.*, vol. 57, no. 2, pp. 169–175, Feb. 1967.

[29] M. Khalighi, N. Schwartz, N. Aitamer, and S. Bourennane, "Fading reduction by aperture averaging and spatial diversity in optical wireless systems," *OSA J. Opt. Commun. Netw.*, vol. 1, no. 6, pp. 580–593, Nov. 2009.

[30] J. H. Churnside, "Aperture averaging of optical scintillations in the turbulent atmosphere," *OSA Appl. Opt.*, vol. 30, no. 15, pp. 1982–1994, May 1991.

[31] L. C. Andrews, R. L. Phillips, and C. Y. Hopen, *Laser Beam Scintillation With Application*. Bellingham, WA, USA: SPIE Press, 2001.

[32] "SBIR investments in optical communications technology 2005 to 2014," *Space communications and navigation*. [Online]. Available: https://www.nasa.gov/sites/default/files/atoms/files/sbir_investments_in_optical_communications_technology.pdf. Accessed on: Oct. 2018.

[33] D. M. Boroson, "Free-Space Optical Communications Comes of Age," MIT Lincoln Laboratory, Photonics Spectra, May 2017. [Online]. Available: https://www.photonics.com/Articles/Free-Space_Optical_Communications_Comes_of_Age/a61909. Accessed on: Oct. 2018.

[34] X. Jin, X. Wang, and C. Y. Hsu, "Design and implementation of mobile free space optical communication system," in *Proc. IEEE Avionics, Fiber-Opt. Photon. Technol. Conf.*, Sep. 2008, pp. 37–38.

[35] J. Akella, C. Liu, D. Partyka, M. Yuksel, S. Kalyanaraman, and P. Dutta, "Building blocks for mobile free-space-optical networks," in *Proc. 2nd IFIP Int. Conf. Wireless Opt. Commun. Netw. (WOCN)*, Mar. 2005, pp. 164–168.

[36] M. Al-Akkoumi, A. Harris, R. Huck, and J. Sluss, "Challenges facing mobile free-space optical communications," *SPIE*, vol. 7324, May 2009, Atmospheric Propagation VI.

[37] M. K. Al-Akkoumi, R. C. Huck, and J. J. Sluss, "High-speed communications enabling real-time video for battlefield commanders using tracked FSO," *Proc. SPIE 6551*, May 2007, Atmospheric Propagation IV, 655105.

[38] G. Oppenhuser, "A world first: Data transmission between European satellites using laser lights," *ESA News, European Space Agency*, Nov. 2001. [Online]. Available: https://www.esa.int/Our_Activities/Telecommunications_Integrated_Applications/A_world_first_Data_transmission_between_European_satellites_using_laser_light. Accessed on: Oct. 2018.

[39] H. Kaushal and G. Kaddoum, "Optical communication in space: Challenges and mitigation techniques," *IEEE Commun. Surveys Tuts.*, vol. 19, no. 1, pp. 57–96, Firstquarter 2017.

[40] "Harnessing light for wireless communications," Jul. 2016. [Online]. Available: https://code.fb.com/connectivity/harnessing-light-for-wireless-communications/. Accessed on: Nov. 2018.

[41] T. Peyronel, K. J. Quirk, S. C. Wang, and T. G. Tiecke, "Luminescent detector for free-space optical communication," *Optica*, vol. 3, no. 7, pp. 787–792, Jul. 2016. [Online]. Available: http://www.osapublishing.org/optica/abstract.cfm?URI=optica-3-7-787

[42] [Online]. Available: https://en.wikipedia.org/wiki/Facebook_Aquila. Accessed on: Dec. 2018.

[43] "Facebook's drones-made in Britain," Jul. 2016. [Online]. Available: https://www.bbc.com/news/technology-36855168 Accessed on: Dec. 2018.

[44] "High altitude connectivity: The next chapter," Jun. 2018. [Online]. Available: https://code.fb.com/connectivity/high-altitude-connectivity-the-next-chapter/ Accessed on: Dec. 2018.

[45] "Using beams of light to support the growing global demand for data," [Online]. Available: https://x.company/projects/fsoc/. Accessed on: Dec. 2018.

[46] "Exploring a new approach to connectivity," Dec. 2017. [Online]. Available: https://blog.x.company/exploring-a-new-approach-to-connectivity-861a0159f63e Accessed on: Nov. 2018.

[47] R. W. DeVaul, E. Teller, C. L. Biffle, and J. Weaver, "Balloon power sources with a buoyancy trade-off," US Patent 2014/0 048 646A1, Feb. 2014.

[48] D. Zou, C. Gong, and Z. Xu, "Secrecy rate of MISO optical wireless scattering communications," *IEEE Trans. Commun.*, vol. 66, no. 1, pp. 225–238, Jan. 2018.

[49] N. Wang, X. Song, J. Cheng, and V. C. M. Leung, "Enhancing the security of free-space optical communications with secret sharing and key agreement," *IEEE/OSA J. Opt. Commun. Netw.*, vol. 6, no. 12, pp. 1072–1081, Dec. 2017.

[50] D. Zou and Z. Xu, "Information security risks outside the laser beam in terrestrial free-space optical communication," *IEEE Photon. J.*, vol. 8, no. 5, Oct. 2016, Art. no. 7804809.

[51] Q. Huang *et al.*, "Secure free-space optical communication system based on data fragmentation multipath transmission technology," *Opt. Exp.*, vol. 26, no. 10, pp. 13 536–13 542, May 2018.

[52] M. Sepantaie, N. Namazi, and A. Sepantaie, "Spectral analysis and implementation of secure chaotic free-space optical communication systems," *Opt. Eng.*, vol. 57, Oct. 2018, Art. no. 106101.

[53] I. S. Gradshteyn and I. M. Ryzhik, *Table of Integrals, Series, and Products*, 7 ed. New York, NY, USA: Academic, 2007.

[54] P. Saxena, A. Mathur, and M. R. Bhatnagar, "Performance of optically pre-amplified FSO system under gamma-gamma turbulence with pointing errors and ASE noise," in *Proc. IEEE 85th Veh. Technol. Conf.*, Jun. 2017, pp. 1–5.

[55] A. Papoulis and S. U. Pillai, *Probability, Random Variables and Stochastic Processes*, 4th ed. TataNew York, NY, USA: McGraw-Hill, 2008.

[56] A. P. Prudnikov, Y. A. Brychkov, and O. I. Marichev, *Integrals and Series*, vol. 3, New York, NY, USA: Gordon and Breach, 1990.

[57] K. Roach, "Meijer-G function representations," in *Proc. ACM Int. Conf. Symbolic Algebraic Comput.*, Jul. 1997, pp. 205–211.

[58] "Meijer G-function." [Online]. Available: https://en.wikipedia.org/wiki/Meijer_G-function. Accessed on: Nov. 2018.

[59] "Trinomial expansion." [Online]. Available: https://en.wikipedia.org/wiki/Trinomial_expansion. Accessed on: Nov. 2018.